Eur. Phys. J. B **27**, 287–297 (2002)
DOI: 10.1140/epjb/e2002-00157-2

THE EUROPEAN PHYSICAL JOURNAL B

Quantum spin dynamics of the bilayer ferromagnet $La_{1.2}Sr_{1.8}Mn_2O_7$

N. Shannon[1,a], T. Chatterji[2], F. Ouchni[3], and P. Thalmeier[4]

[1] Max–Planck–Institut für Physik komplexer Systeme, Nöthnitzer Str. 38, 01187 Dresden, Germany
[2] Institut Laue-Langevin, BP 156, 38042 Grenoble Cedex 9, France
[3] Institut für Theoretische Physik III, Universität Stuttgart, Pfaffenwaldring 57, 70550 Stuttgart, Germany
[4] Max-Planck-Institut für Chemische Physik fester Stoffe, Nöthnitzer Str. 40, 01187 Dresden, Germany

Received 15 January 2002
Published online 6 June 2002 –

Abstract. We construct a theory of spin wave excitations in the bilayer manganite $La_{1.2}Sr_{1.8}Mn_2O_7$ based on the simplest possible double–exchange model, but including leading quantum corrections to the spin wave dispersion and damping. Comparison is made with recent inelastic neutron scattering experiments. We find that quantum effects account for some part of the measured damping of spin waves, but cannot by themselves explain the observed softening of spin waves at the zone boundary. Furthermore a doping dependence of the total spin wave dispersion and the optical spin wave gap is predicted.

PACS. 75.30.DS Spin waves – 75.25.+z Spin arrangements in magnetically ordered materials (including neutron and spin-polarized electron studies, synchrotron-source X-ray scattering, etc.)

1 Introduction

The colossal magnetoresistance (CMR) manganites, of which perhaps the best known is $La_{1-x}Ca_xMnO_3$, have been challenging the theoretical understanding of the way in which magnetism and metallic behaviour co–exist for more than fifty years. These materials are difficult to describe for precisely the very same reason that they are interesting; namely that they exhibit a complex interplay between lattice, charge, orbital and spin degrees of freedom. This gives rise to a very rich phase diagram, exhibiting different magnetic, orbital and charge orders, and both metallic and insulating behaviour as a function of temperature, pressure, applied field and doping [1–3]. Even within the "simple" low temperature ferromagnetic phase, the mechanism for the metal–insulator transition which occurs as ferromagnetic order breaks down remains controversial.

The CMR manganites share a layered perovskite structure with the even more widely studied high-temperature (HT_c) superconductors; they may be synthesised with one, two, three (or many), neighbouring conducting planes. The materials most frequently discussed are the three dimensional "infinite layer" compounds, which have equally spaced planes and are approximately cubic in symmetry. Here we will construct a theory for ferromagnetism in $La_{2-2x}Sr_{1+2x}Mn_2O_7$ and discuss results especially for $x = 0.4$. In this bilayer compound planes of magnetic Mn atoms in MnO_6 octahedra are grouped in well separated pairs. The small spin wave dispersion found empirically perpendicular to these planes provides us with a justification for considering, as a first approximation, only a single pair of planes *i.e.* a single ferromagnetic bilayer with moments lying in the *ab*-plane [3,4]. The T–x phase diagram and evolution of magnetic structure with doping has been reported in [5–8] and a FM phase persists in the range $0.3 \leq x \leq 0.4$. For larger doping an intra– bilayer canting of moments appears and the charge ordered stoichiometric compound ($x = 0.5$) $LaSr_2Mn_2O_7$ finally is an AF insulator. Here we will concentrate on predictions for the spin wave dispersion and damping of FM bilayer manganites which have been measured by inelastic neutron scattering [9–14,8]. Calculation of the spin wave damping requires going beyond the usual semi–classical picture used to describe spin wave excitations in the manganites to include quantum effects. In Section 2 we present a minimal model of a bilayer manganite based on Zener's double exchange (DE) mechanism [15,16]. A fully quantum mechanical large S expansion of this model is developed, following a recently introduced operator expansion method [17–20]. Predictions for the dispersion of the optical and acoustic spin wave modes of a double exchange bilayer, their doping dependence together with their damping, are made in Section 3. A comparison with experimental data for $La_{1.2}Sr_{1.8}Mn_2O_7$ is made in Section 4. This comparison

[a] e-mail: shannon@mpipks-dresden.mpg.de

provides a test of how well the DE model describes FM in CMR materials when quantum effects are included. We conclude in Section 5 with a discussion of the implications of our results for the theory of ferromagnetism in CMR manganites.

2 The model Hamiltonian

In this section we consider $La_{1.2}Sr_{1.8}Mn_2O_7$, as a concrete example of a bilayer DE system, and derive a model Hamiltonian for a single $La_{1.2}Sr_{1.8}Mn_2O_7$ bilayer starting from Zener's DE mechanism, in the limit where the strength of the Hund's rule coupling is taken to be infinite. The comparison of the predictions of this model with experimental data in Section 4 therefore provide a test of how well the DE model describes FM in CMR materials. The crystal structure of $La_{2-2x}Sr_{1+2x}Mn_2O_7$ belongs to the space group I4/mmm with a body centred tetragonal conventional unit cell that contains two distorted MnO_6 octahedra, whose distortion depends on doping [5,6]. The lattice constants are $a = 3.87$ Å and $c = 20.14$ Å. The intra– bilayer spacing $d \simeq a$ is much smaller than the distance $D = 6.2$ Å between two adjacent bilayers. Therefore bilayers are well separated, and the spin wave spectrum measured by inelastic neutron scattering indeed shows a very small dispersion of about 0.4 meV in the direction perpendicular to the planes [9,21]. For this reason we will neglect coupling between the planes entirely, and model $La_{1.2}Sr_{1.8}Mn_2O_7$ in terms of a single pair of layers. Within a given bilayer, both magnetism and metallic behaviour originate in the Mn d–electrons. Mn t_{2g} d–orbitals are exactly half filled, and form a spin 3/2 local moment because of strong Hund's rule coupling. This local moment couples to itinerant electron e_g d–orbitals through a similar Hund's rule exchange interaction. In the metallic phases of the manganites, electrons in e_g orbitals delocalise by hopping between Mn atoms through intermediate O_{2p} orbitals — a process named "double exchange" by Zener [15]. This delocalisation of the e_g electrons stabilises FM order among the t_{2g} spins, since both are strongly coupled by Hund's rule interaction, and the e_g electrons will have the maximum kinetic energy if all t_{2g} spins are aligned.

In the bilayer compounds the MnO_6 octahedra show a doping dependent pronounced Jahn-Teller (JT) distortion [5,6], therefore Mn^{3+} site symmetry is no longer cubic and a crystalline electric field (CEF) splitting of e_g ($d_{3z^2-r^2}$, $d_{x^2-y^2}$) states ensues. The influence of this splitting on the stability of magnetic phases was investigated by Okamoto *et al.* [6]. The e_g splitting energy Δ is generally smaller than the inter-site in–plane hopping t and therefore in the FM ground state the orbital state is of uniformly mixed $d_{3z^2-r^2}/d_{x^2-y^2}$ character. In this case orbital degrees of freedom do not appear explicitly in the Hamiltonian but the degree of admixture determines the ratio of interlayer ($t_\perp$) to intra–layer hopping (t) of the effective single band (orbital) Hamiltonian which is then given by

$$\mathcal{H}_{DE} = -t \sum_{\langle ij\rangle\lambda\alpha} c^\dagger_{i\lambda\alpha} c_{j\lambda\alpha} - t_\perp \sum_{i\alpha} \left\{ c^\dagger_{i1\alpha} c_{i2\alpha} + \text{h.c.} \right\} - \frac{J_H}{2} \sum_{i\lambda\alpha\beta} \boldsymbol{S}_{i\lambda} \cdot c^\dagger_{i\lambda\alpha} \boldsymbol{\sigma}_{\alpha\beta} c_{i\lambda\beta} \quad (1)$$

where $c^\dagger_{\lambda i\alpha}$ is the creation operator for an e_g electron on site i of plane $\lambda = \{1, 2\}$ with spin $\alpha = \{\uparrow, \downarrow\}$. The components of the operator $\boldsymbol{\sigma}_{\alpha\beta}$ are Pauli matrices, and $\boldsymbol{S}_{i\lambda}$ is the spin operator for the t_{2g} electrons on that site. The on-site exchange J_H parameterises Hund's rule coupling, and the sum $\langle ij\rangle$ runs over nearest neighbours within a plane. Our subsequent DE spin wave analysis will lead to $t \simeq 0.175$ eV and $t_\perp \simeq 0.1$ eV. This is much smaller than the intra-atomic (Hund's rule) exchange $J_H \sim 2$ eV which may be estimated from the splitting of majority and minority spin LDA bands in the stoichiometric ($x = 0.5$) compound [22].

In addition, there may be super-exchange interactions between spins, both within the plane (J) and between the two planes of the bilayer ($J_\perp$). These can be parameterised by

$$\mathcal{H}_{EX} = -J^{EX} \sum_{\langle ij\rangle\lambda} \boldsymbol{T}_{i\lambda} \cdot \boldsymbol{T}_{j\lambda} - J^{EX}_\perp \sum_i \{\boldsymbol{T}_{i1} \cdot \boldsymbol{T}_{i2} + \text{h.c.}\} \quad (2)$$

where $\boldsymbol{T}_{i\lambda} = \boldsymbol{S}_{i\lambda} + 1/2 \sum_{\alpha\beta} c_{i\lambda\alpha} \boldsymbol{\sigma}_{\alpha\beta} c_{i\lambda\beta}$ is the total spin operator for both t_{2g} and e_g d–electrons on the site $i\lambda$. Exchange integrals in the manganites can be FM or antiferromagnetic (AF) depending on the details of orbital occupancy and electronic structure.

To evaluate the spectrum, or even to find the ground state of the Hamiltonian equation (1) is a formidable task, but if we assume FM order and treat the length of the local moment S, and the ratio J_H/t as large parameters, we can derive a controlled expansion of the properties of a bilayer ferromagnet. A number of ways of performing this large S expansion have been suggested (see *e.g.* [23–25]). Each of these have their advantages, but in the case in point, it is most convenient to work with eigenstates of the Hund's rule coupling term, and to quantize small fluctuations of the total spin operator $\boldsymbol{T}_{i\lambda}$ using a generalization of the usual Holstein–Primakoff procedure due to Shannon and Chubukov [17,18]. A non–technical introduction to this method is given in [20]. Technical details, including a discussion of its relationship to other approaches are given in [19]. We now generalize the method to a bilayer system. In the limit $t/J_H \ll 1$, $t_\perp/J_H \ll 1$ J_H we obtain a model in which bosonic fluctuations of the total spin interact with a band of spinless electrons. In this limit it makes sense first to diagonalise the Hund's rule coupling term in the Hamiltonian and then to introduce the hopping of electrons as a "perturbation". We do this following the method introduced in [17] by constructing new Fermi operators $\{f, f^\dagger\} = 1$ and $\{p, p^\dagger\} = 1$ which create eigenstates of the Hund's rule coupling term with eigenvalue

$-J_H S/2$ and $J_H(S+1)/2$, respectively. The Hund's rule coupling then reads

$$-\frac{J_H S}{2}\left[f^\dagger f - \left(1+\frac{1}{S}\right)p^\dagger p + \frac{f^\dagger f p^\dagger p}{S}\right] \tag{3}$$

where the sum over sites has been suppressed. In the physically relevant limit $J_H \to \infty$, for less than half filling, we can remove p Fermions from the problem entirely, and rewrite the kinetic energy term in equation (1) entirely in terms of a band of spinless (f) electrons interacting with fluctuations of the total spin parameterised by the Bose operators $[\tilde{a}, \tilde{a}^\dagger] = 1$.

To accomplish this transcription of the Hamiltonian it is sufficient to know a few of the leading terms of the inverse transformation between $c_\uparrow$ and $c_\downarrow$ electron operators, and the new f operators creating eigenstates of the Hund's rule coupling term

$$c_\uparrow = f\left(1 - \frac{\tilde{a}^\dagger \tilde{a}}{4S}\right) + \ldots \tag{4}$$

$$c_\downarrow = \frac{f\tilde{a}^\dagger}{\sqrt{2S}}\left(1 - \frac{1}{2S}\right) + \ldots \tag{5}$$

To prove this result, and to derive the full transformation between "laboratory frame" $c_\uparrow$ and $c_\downarrow$ electron operators and the "local frame" f and p operators, together with the appropriate algebra for the spin boson $\tilde{a}$ is an involved task. We will not discuss the transformation in detail here (see [20]), but note that all the necessary canonical commutation and anticommutation relations, *e.g.* $[f, \tilde{a}] = 0$, *etc.*, are obeyed.

Up to a constant the transformed DE Hamiltonian reads

$$\mathcal{H} = \mathcal{H}_0 + \mathcal{V}_2 + \mathcal{O}(1/S^3) \tag{6}$$

where the kinetic energy term for f electrons is

$$\mathcal{H}_0 = -t\sum_{\langle ij\rangle\lambda} f^\dagger_{i\lambda} f_{j\lambda} - t_\perp \sum_i \left\{ f^\dagger_{i1} f_{i2} + \text{h.c.}\right\}. \tag{7}$$

At this level the spin excitations $\tilde{a}$ are dispersionless. Spin wave dispersion first enters into the problem through interaction at $\mathcal{O}(1/S)$ through the interaction term

$$\begin{aligned}\mathcal{V}_2 = &-\frac{t}{4S}\sum_{\langle ij\rangle\lambda} f^\dagger_{i\lambda} f_{j\lambda}\left[\left(\tilde{a}^\dagger_{j\lambda}\tilde{a}_{j\lambda} + \tilde{a}^\dagger_{i\lambda}\tilde{a}_{i\lambda}\right)\left(1-\frac{3}{8S}\right)\right.\\ &\left.-2\tilde{a}^\dagger_{i\lambda}\tilde{a}_{j\lambda}\left(1-\frac{1}{2S}\right)\right]\\ &-\frac{t_\perp}{4S}\sum_i\left\{f^\dagger_{i1}f_{i2}\left[\left(\tilde{a}^\dagger_{i1}\tilde{a}_{i1} + \tilde{a}^\dagger_{i2}\tilde{a}_{i2}\right)\left(1-\frac{3}{8S}\right)\right.\right.\\ &\left.\left.-2\tilde{a}^\dagger_{i1}\tilde{a}_{i2}\left(1-\frac{1}{2S}\right)\right] + \text{h.c.}\right\}\end{aligned} \tag{8}$$

where we have neglected a further four boson vertex at $\mathcal{O}(1/S^2)$ which is irrelevant at zero temperature.

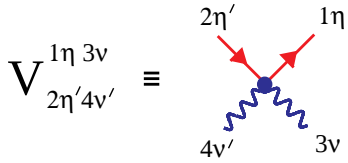

Fig. 1. Convention for labelling vertex for interaction between electrons and spin waves in the limit $J_H/t \to \infty$. Straight lines correspond to electrons $f_{k\eta}$ and wavy lines to spin waves $\tilde{a}_{q\nu}$, where k and q are momenta in–plane and $\eta, \nu = 0, \pi$ are the momenta out of plane.

By Fourier transformation we obtain the following Hamiltonian which describes a band of spinless electrons interacting with (initially dispersionless) bosonic spin–wave excitations.

$$\begin{aligned}\mathcal{H} &= \mathcal{H}_0 + \mathcal{V}_2 + \mathcal{O}(1/S^3)\\ \mathcal{H}_0 &= \sum_k \left(\epsilon_k - t_\perp\right) f^\dagger_{k0} f_{k0} + \left(\epsilon_k + t_\perp\right) f^\dagger_{k\pi} f_{k\pi}\\ \mathcal{V}_2 &= \frac{1}{N}\sum_{k_1\cdots k_4}\sum_{\eta\eta'\nu\nu'=\{0,\pi\}} \mathcal{V}^{1\eta 3\nu}_{2\eta' 4\nu'} f^\dagger_{1\eta} f_{2\eta'} \tilde{a}^\dagger_{3\nu}\tilde{a}_{4\nu}\\ &\quad\times \delta_{1+3-2-4}\delta_{\eta+\nu-\eta'-\nu'}\end{aligned} \tag{9}$$

where we consider symmetric and antisymmetric combinations of electron operators (binding and antibinding bands), and of spin operators (acoustic and optical spin waves), for the two planes. For the simple nearest neighbour tight–binding model equation (1) the in–plane electronic dispersion is given by $\epsilon_k = -\,\text{zt}\frac{1}{2}(\cos k_x + \cos k_y)$ in units where the distance between Mn atoms $a = 1$. The scale of interaction between electrons and spin waves $\mathcal{V}_2$ is determined entirely by electronic energies, but is one order in S down on the kinetic energy term $\mathcal{H}_0$. There are a total of eight physically distinct vertices (decay channels) for interaction between electrons and spin excitations. The convention for labelling these vertices is shown in Figure 1 and their algebraic expressions are given in equations (A.1) and (A.2). The spin wave dispersion is now determined by the leading order self energy up to $1/S^2$ shown in Figure 2. We first discuss the results within the usual semiclassical ($1/S$) approximation.

3 Theoretical predictions

In a cubic system, at a semi–classical level of approximation, Zener's DE mechanism leads to a FM effective nearest neighbour Heisenberg exchange interaction between neighbouring Mn spins, with a spin wave dispersion

$$\omega_q = zJ^{DE}S[1-\gamma_q] \tag{10}$$

where the size of the effective exchange interaction is set by electron energies [16]

$$J^{DE} = \frac{1}{2S^2}\frac{t}{N}\sum_k \gamma_k n(k). \tag{11}$$

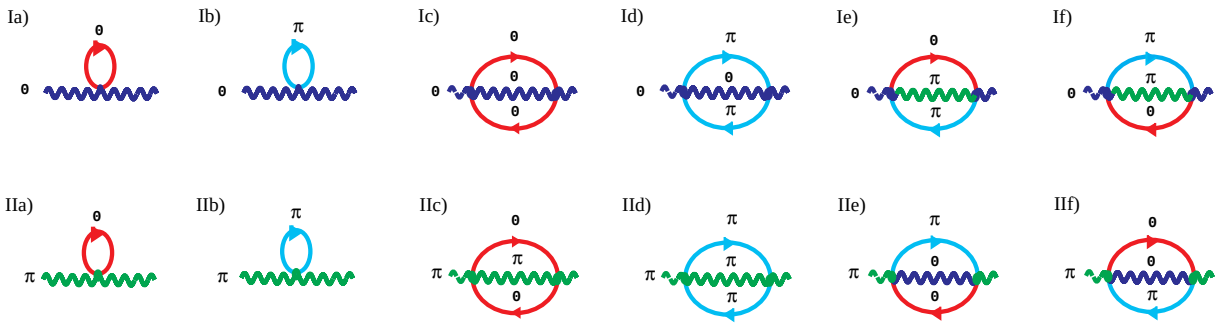

Fig. 2. Leading self energy corrections for spin waves due to interaction with electrons in limit $J_h/t \to \infty$. Diagrams Ia–f) show contributions for acoustic ($\tilde{a}_{q0}$) and diagrams IIa–f) optical ($\tilde{a}_{q\pi}$) spin wave modes.

Here $\gamma_q = \frac{1}{3}(\cos q_x + \cos q_y + \cos q_z)$ is the structure factor for a 3D cubic lattice and $n(k)$ is the occupation of the electronic state with momentum k, and J^{DE} is proportional to the expectation value of the kinetic energy operator per Mn–Mn bond, relative to the center of the band. Spin waves are exact eigenstates of a Heisenberg FM, and therefore undamped. This simple mapping between DE and Heisenberg models breaks down, however, when quantum effects are included [17,18].

The situation in a bilayer system is complicated in that there are both optical and acoustic branches of spin wave excitations, but the mapping onto an effective Heisenberg model is once again possible at a semi–classical level. Evaluating the effect of interaction between electrons and spin waves described by equation (9) to $\mathcal{O}(1/S)$, and now including the effect of super–exchange terms, we obtain a spectrum:

$$\begin{aligned}\omega_q^0 &= z\left(J^{DE} + J^{EX}\right) S\left[1-\gamma_q\right] \\ \omega_q^\pi &= z\left(J^{DE} + J^{EX}\right) S\left[1-\gamma_q\right] \\ &\quad +2\left(J_\perp^{DE} + J_\perp^{EX}\right) S \end{aligned} \tag{12}$$

where in 2D $\gamma_q = \frac{1}{2}(\cos q_x + \cos q_y)$, ω_q^0 is the dispersion of the acoustic and ω_q^π the dispersion of the optical spin wave branch. The size of the DE in-plane contribution to the effective exchange integral is once again set by the expectation value of the kinetic energy on a single bond, and the DE between the two planes is determined by the occupation difference of binding and antibinding bands:

$$\begin{aligned} J^{DE} &= \frac{1}{2S^2}\frac{t}{2N}\sum_k \gamma(k)\left[n_0(k) + n_\pi(k)\right] \\ J_\perp^{DE} &= \frac{1}{2S^2}\frac{t_\perp}{2N}\sum_k \left[n_0(k) - n_\pi(k)\right]. \end{aligned} \tag{13}$$

Here we used the occupation numbers $n_0(k) = \langle f_{k0}^\dagger f_{k0}\rangle$ and $n_\pi(k) = \langle f_{k\pi}^\dagger f_{k\pi}\rangle$ of the binding and antibinding electron bands $\epsilon_0(k) = -t_\perp + \epsilon(k)$, $\epsilon_\pi(k) = t_\perp + \epsilon(k)$ respectively. Our result at this order agrees perfectly with earlier calculations of the spin wave spectrum in a bilayer [9,10]. The effective exchange constants in equation (13) can be evaluated as function of the doping x which gives the number of holes per Mn-site or the total number of e_g electrons per Mn site $n = n_0 + n_\pi = 1 - x$ that occupy the 0, π-bands. By using the DOS functions $N_{0,\pi}(\epsilon) = N(\epsilon \pm t_\perp)$, the electron number $\mathrm{n}_{0,\pi}$ and the average band energy $\epsilon_{0,\pi}$ of the 2D binding and antibinding bands respectively may be expressed as

$$\begin{aligned} n_{0,\pi} &= \int_{-W}^{\epsilon_F \pm t_\perp} N(\epsilon)\mathrm{d}\epsilon \\ \epsilon_{0,\pi} &= \int_{-W}^{\epsilon_F \pm t_\perp} N(\epsilon)\epsilon\mathrm{d}\epsilon \\ N(\epsilon) &= \frac{2}{\pi^2}\frac{1}{W}K\left(\left[1-\left(\frac{\epsilon}{W}\right)^2\right]^{\frac{1}{2}}\right). \end{aligned} \tag{14}$$

Here $W = zt$ and $2W$ is the band width of of each of the 2D bands $\epsilon_{0,\pi}(k)$ and ϵ_F is the Fermi level. Furthermore $K(\xi)$ is the complete elliptic integral of the first kind. The total DOS $N_t = N_0 + N_\pi$ and the total number of electrons n as a function of the Fermi level is shown in the inset of Figure 3. The spikes in the DOS are logarithmic singularities of each of the 2D bands at its band center ($\pm t_\perp$). We then obtain for the effective DE exchange constants after equation (13):

$$\begin{aligned} J^{DE} &= -\frac{1}{2S^2}\frac{1}{2z}(\epsilon_0 + \epsilon_\pi) \\ J_\perp^{DE} &= \frac{1}{2S^2}\frac{t_\perp}{2}(n_0 - n_\pi). \end{aligned} \tag{15}$$

The DE anisotropy ratio $J_\perp^{DE}/J^{DE}$ is is equal to the ratio $\omega_0^\pi / W_{sw}^{[110]}$ of optical spin wave gap $\omega_0^\pi = 2SJ_\perp^{DE}$ to the acoustical (or optical) spin wave band width $W_{sw}^{[110]} = 2zSJ^{DE}$ along [110] direction and it is given by

$$\frac{J_\perp^{DE}}{J^{DE}} = -\left(\frac{t_\perp}{t}\right)\frac{W\left(n_0 - n_\pi\right)}{\epsilon_0 + \epsilon_\pi}. \tag{16}$$

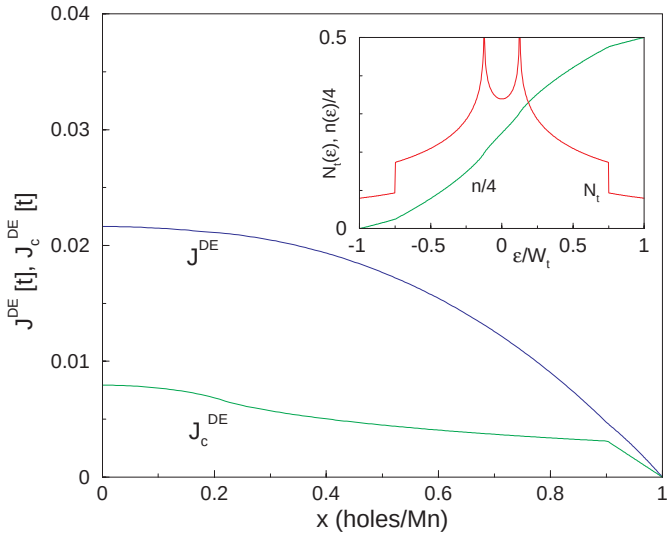

Fig. 3. Inset shows total DOS $N_t(\epsilon) = N_0(\epsilon)+N_\pi(\epsilon)$ and total electron number n for the 2D bands $\epsilon_0(k)$ and $\epsilon_\pi(k)$ $W_t = W + t_\perp$ is half of the overall bandwidth. Main figure shows variation of J^{DE} and $J_c^{DE} \equiv J_\perp^{DE}$ with hole doping under the assumption that $t_\perp/t = 0.57$ (fixed for $x = 0.4$) is *independent* of x. The physical FM regime is restricted to $0.3< x <0.4$.

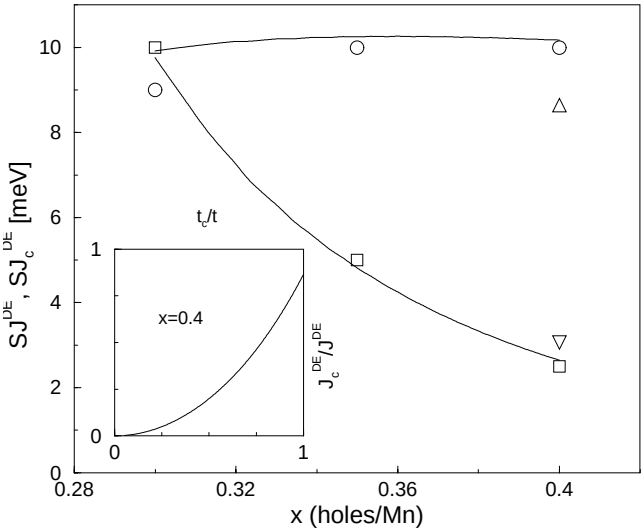

Fig. 4. Doping dependence of DE exchange constants. The strong reduction of $J_c^{DE} \equiv J_\perp^{DE}$ with increasing x is due to the strong reduction of $t_c \equiv t_\perp$ due to the JT effect of MnO units as described by equation (17) with $\Omega_\perp\eta_\perp = -2$. Experimental data from [14] (circles, squares) and [10] (triangles). In the latter case a somewhat smaller $SJ^{DE} = 8.6$ meV was obtained by fitting the spin wave stiffness constant in contrast to the value of 10 meV obtained by fitting to the whole spin wave bandwidth $W_{sw}^{[100]} = zSJ^{DE}$. The inset shows the dependence of DE exchange anisotropy on the hopping anisotropy for a fixed doping $x = 0.4$.

For $t_\perp \ll t$ the occupation number difference increases linearly in $t_\perp$, and using equation (16) we find $J_\perp^{DE}/J^{DE} \sim (t_\perp/t)^2$, as shown in the inset of Figure 4. Numerical values from equation (15) are presented in Figure 3 as function of the doping $x = 1 - n$. It shows the variation for the model DE for fixed $t_\perp$ in the whole range $0\leq x \leq 1$ although it must be kept in mind that the physical region for the FM phase of $La_{2-2x}Sr_{1+2x}Mn_2O_7$ is much smaller, according to [5] it exists for $0.3\leq x \leq 0.4$. From a comparison of the experimental values of the optical spin wave gap and the spin wave band width at $x = 0.4$ with equation (15) and with the insert in Figure 4 we can obtain estimates for the underlying microscopic model parameters within the classical approximation, namely $t_\perp/t \simeq 0.57$ corresponding to the experimental $J_\perp^{DE}/J^{DE} \simeq 0.30$ at low temperature and $t \simeq 0.175$ eV ($t_\perp = 0.1$ eV) as obtained from the experimental value $SJ^{DE} = 10$ meV (from $W_{sw}^{[100]} = zSJ^{DE} = 40$ meV [11]) by using equation (15). According to Figure 3 $J^{DE}(x)$ and $J_\perp^{DE}(x)$ should not change dramatically with the hole doping in the FM regime $0.3 \leq x \leq 0.4$, namely at most 6% and 15% respectively. However this refers to the artificial situation where $t_\perp$ does not depend on the doping. From the experimental investigation of optical spin wave gap and dispersion for various dopings $x = 0.30$, $x = 0.35$ and $x = 0.40$ [14] it is known that indeed J^{DE} shows no change in this region, however $J_\perp^{DE}(x)$ strongly increases by a factor of four when the doping is reduced from $x = 0.4$ to $x = 0.3$.

The origin of this pronounced doping dependence of interlayer DE is connected to the large Jahn-Teller(JT) distortion observed [5] in the bilayer manganites. This distortion is defined as Δ_{JT} = apical Mn-O bond length/equatorial bond length. Decreasing the doping leads to an increase of Δ_{JT}. The driving mechanism for this JT distortion is an increasing admixture of $d_{3z^2-r^2}$ states into the conduction band states which naturally leads to an increase of $t_\perp$ with reduced doping, which in turn strongly increases the interlayer $J_\perp^{DE}(x)$ as shown in the inset of Figure 4. For the limited FM doping range one may describe this dependence by introducing dimensionless Grüneisenparameters $\eta_\perp = -(\partial \ln D/\partial \ln x)$ and $\Omega_\perp = -(\partial \ln t_\perp/\partial \ln D)$ where D = distance between the layers of a single bilayer. They describe the doping dependence of the JT-distortion and the distortion dependence of the interlayer- hopping respectively. The JT effect on the intra-layer hopping t is neglected since no doping dependence of J^{DE} is observed. Assuming that $\eta_\perp$ and $\Omega_\perp$ are constants in the range of x considered, this amounts to a doping dependence of $t_\perp$ given by

$$t_\perp(x) = t_\perp^0 \left(\frac{x}{x_0}\right)^{\Omega_\perp\eta_\perp} \qquad (17)$$

where *e.g.* $x_0 = 0.4$ and $t_\perp^0 = t_\perp(x_0)$. According to the physical origin of the JT distortion mentioned above one has to expect that $\Omega_\perp\eta_\perp < 0$. Using the above relation in equation (15) with $\Omega_\perp\eta_\perp = -2$ one obtains the doping dependence of the exchange constants shown in Figure 4 together with the experimental values for various dopings. Using $\eta_\perp \simeq 0.037$ from the JT-distortions given in [5] one

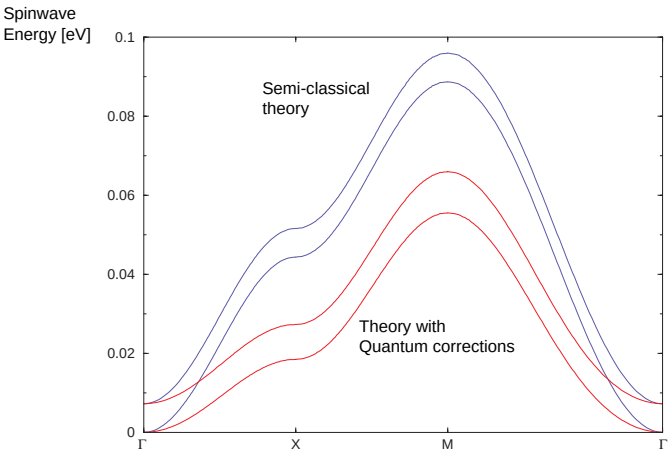

Fig. 5. Spectrum for optical and acoustic spin wave modes throughout the Brillouin zone, calculated for doping $x = 0.4$, $t = 0.175$ eV, $t_\perp = 0.1$ eV. Upper pair of lines – semi–classical spin wave dispersion at $\mathcal{O}(1/S)$; lower pair of lines – spin wave spectrum including quantum effects at $\mathcal{O}(1/S^2)$.

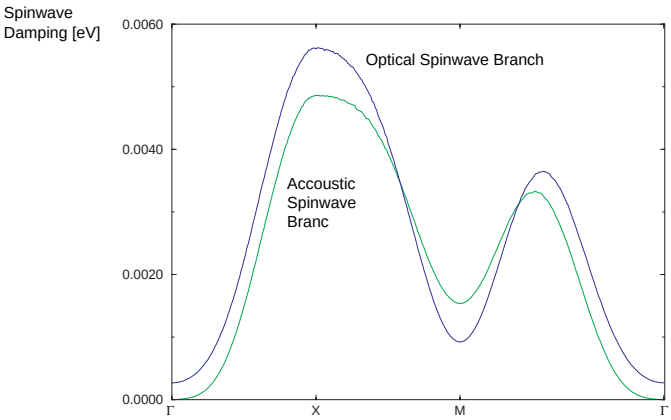

Fig. 6. Damping of acoustic and optical spin wave modes, throughout the Brillouin Zone, calculated for doping $x = 0.4$, $t = 0.175$ eV, $t_\perp = 0.1$ eV.

then obtains from the above relation $\Omega_\perp \simeq -54$. This large negative Grüneisenparameter characterises a strong dependence of the effective interlayer hopping $t_\perp$ on the layer spacing D within a bilayer. The JT-distortion increases with temperature for constant doping implying an increase of $t_\perp$ and hence $J_\perp^{DE}$. The DE therefore becomes less anisotropic at higher temperature. This has indeed been observed for $x = 0.4$ in diffuse neutron scattering where $J_\perp^{DE}/J^{DE} \simeq 0.5$ has been found at room temperature [26] compared to $J_\perp^{DE}/J^{DE} \simeq 0.3$ from the low temperature spin wave experiments discussed here [27].

The results for the dispersion of acoustic and optic spin wave modes for throughout the Brillouin zone, at a semi–classical level and for the parameters given above are shown in Figure 5. At zero temperature, at a semi–classical level, spin waves are undamped, *i.e.* states with a single spin wave excitation are good eigenstates of the Hamiltonian, with no allowed decay processes. The dispersion of spin waves is generated by their *elastic* scattering by the average density of electrons. At $\mathcal{O}(1/S^2)$ spin waves can decay through interaction with electrons into lower energy spin excitations dressed with particle hole pairs – an inelastic process. This leads to a damping of spin waves, and a corresponding shift in spin wave dispersion to lower energy. We can evaluate both effects starting from the Hamiltonian equation (9). We consider

$$\begin{aligned} \bar{\omega}_q^\nu &= \omega_q^\nu + \mathrm{Re}\{\Sigma^\nu(q,0)\} \\ \gamma_q^\nu &= -\mathrm{Im}\{\Sigma^\nu(q,\omega_q^\nu)\} \end{aligned} \tag{18}$$

where $\bar{\omega}_q^\nu$ is the net dispersion and γ_q^ν the damping of the spin wave excitation, and $\Sigma^\nu(q,\Omega)$ is the momentum and frequency dependent selfenergy correction due to interaction of spin waves with electrons at $\mathcal{O}(1/S^2)$. The various contributions to the spin wave selfenergy are shown in Figure 2 at this order and given in Appendix A. The new physical process involved is the *inelastic* scattering of spin waves from fluctuations of charge density. Results for spin wave dispersion, including leading quantum corrections are shown in Figure 5, and values for the damping of spin waves in Figure 6. These should be compared with results for a single layer quoted in [28]; for $t_\perp \to 0$ the two theories are essentially equivalent.

The immediate conclusion which we can draw from these calculations is that quantum effects on spin waves in a DE bilayer are very large. The downward renormalisation of spin wave dispersion at $\mathcal{O}(1/S^2)$ is a sizable fraction (about 30%) of the spin wave dispersion at $\mathcal{O}(1/S)$. Similarly, the damping of spin waves is quite pronounced, being of the scale 5–10% of the spin wave dispersion, rising to a maximum value ~ 6 meV at the zone boundary. Because of the large renormalisation of the spin wave spectrum at $\mathcal{O}(1/S^2)$ it would be necessary to reparameterise our model to fit experimental data with the leading quantum effects included, by increasing the sizes of the hopping integrals t and $t_\perp$, and including superexchange interactions J^{EX} and $J_\perp^{EX}$. Any increase in the electron bandwidth would give a proportionate increase in the damping of spin waves.

Examining the quantum corrections in more detail, we find that the spin wave dispersion has been modified so as to give a relative softening of spin wave modes near the zone center. This can be understood loosely in terms of the dynamical generation of an effective non nearest–neighbour couplings between spins by processes $\mathcal{O}(1/S^2)$. It is also interesting to note that the gap between acoustic and optical modes is now momentum dependent.

While these effects are of themselves interesting, they do not offer any unambiguous signatures of quantum effects in the magnetism of $La_{2-2x}Sr_{1+2x}Mn_2O_7$, as one could achieve similar modifications of the spin wave dispersion simply by postulating additional exchange couplings between spins on an *ad hoc* basis. It is the damping of spin waves at zero temperature which sharply

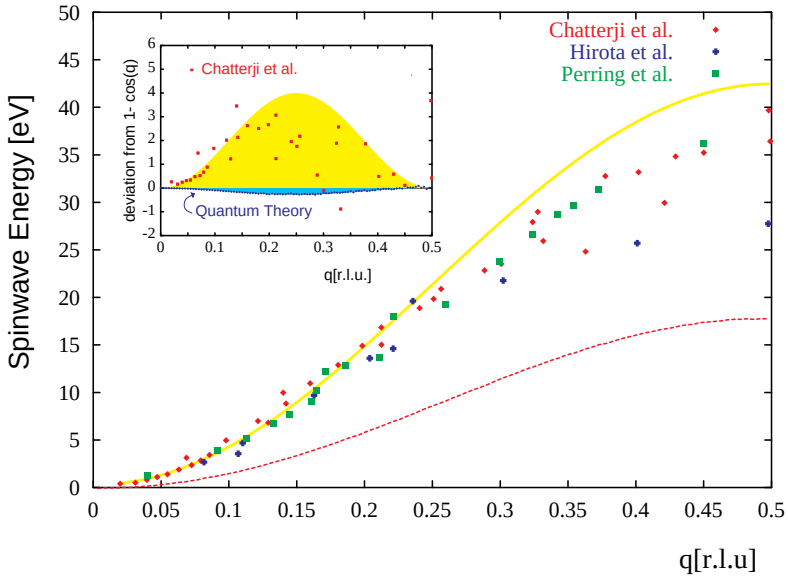

Fig. 7. Dispersion of the acoustic spinwave branch of $La_{1.2}Sr_{1.8}Mn_2O_7$ in the [100] direction, as measured by Chatterji *et al.* [11] (diamonds), Hirota *et al.* [8] (crosses) and Perring *et al.* [14] (squares), together with an semi–classical extrapolation of a fit to the spin stiffness in the zone center (solid line) and the prediction based on equation (1) with quantum effects included (dashed line). Inset – deviations from simple $1-\cos(q_x)$ form of dispersion predicted by semi–classical analysis, for experimental data (Chatterji *et al.* [11] – squares), and for the DE model including quantum fluctuations (circles). The shaded area is a guide to the eye.

distinguishes a DE system from any conceivable Heisenberg ferromagnet. In a the Heisenberg ferromagnet, spin waves are undamped at zero temperature, and damping only becomes appreciable for temperatures large compared with the spin stiffness D.

The damping which we predict for the DE model equation (1) at zero temperature is large and highly momentum dependent. The zone centre acoustic mode must remain undamped (in the absence of any magnetic anisotropy) as it is the Goldstone mode of the system. Accordingly, in the zone centre, we find that the damping of the acoustic mode vanishes as

$$\Gamma_q^{AC} = \alpha^{AC} q^5. \tag{19}$$

The optical spin waves are not Goldstone modes, however, and have a finite dispersion (and damping) in the zone centre. We find that the latter behaves as

$$\Gamma_q^{OP} = \Gamma_0^{0P} + \alpha^{OP} q^3. \tag{20}$$

The lower power law in q here reflects the way in which the vertex for spin wave scattering is cut off by the interlayer hopping $t_\perp$.

Away from the zone centre the spin wave damping exhibits stationary points at the symmetry points of the Brillouin zone – a maximum for both acoustic and optic modes at X, and a minimum for both at M. It is interesting to note that the higher energy optic modes are not always more strongly damped than the acoustic modes, and that the maximum damping does not occur for the highest spin wave energies, as one might expect. In fact the momentum dependence of the damping of spin waves in DE systems varies strongly with doping, being constrained by both the geometry of the Fermi surface and the complex momentum dependence of the spin wave scattering vertex.

4 Comparison with experiment

The spin wave dispersions in bilayer manganites have been investigated by several groups [8–14], and a consensus was reached that the data could not be explained using a nearest neighbour Heisenberg model dispersion of the form equation (12) [8,10–12]. A representive selection of experimental data for the dispersion of the acoustic spinwave mode in the [100] direction for $La_{1.2}Sr_{1.8}Mn_2O_7$ is shown in Figure 7. The dispersion expected for a nearest neighbour Heisenberg model would be of the form $(zJS/2)[1-\cos(q_x)]$, where $2zJS = 8JS$ is the total bandwidth of the acoustic spinwave branch.

In the inset to Figure 7, we illustrate the departure from nearest neighbour Heisenberg model behaviour seen in experiment by subtracting from the measured points $(\omega_X/2)[1-\cos(q_x)]$ where ω_X is the value of spinwave dispersion for the acoustic branch at $\boldsymbol{q} = (0.5, 0, 0)$. It can clearly be seen that corrections to the expected semi–classical behaviour, defined in this way, are positive. The shaded area (a guide to eye) gives some idea of the effect of a next nearest neighbour Heisenberg coupling on the dispersion in this direction.

Departures from nearest neighbour Heisenberg model behaviour have also been observed in many (pseudo-)cubic manganite systems, for example $Pr_{0.63}Sr_{0.37}MnO_3$ [29]. Typically, what has been seen in both cubic and bilayer systems is a softening and broadening of the zone boundary spin waves. The total spin wave bandwidth measured to the zone boundary is much less than would be predicted on the basis of the spin stiffness D measured in the zone center.

In the case of the bilayer system $La_{1.2}Sr_{1.8}Mn_2O_7$, the dispersion of the acoustic mode near the zone center has the form

$$\omega_q^0 = \Delta + D^0 q^2 \tag{21}$$

with $\Delta \ll D^0$, as would be expected for a FM with small magnetic anisotropy. If we compare this with the measured total acoustic spin wave bandwidth, as defined by the spin wave energy at the zone boundary [11], it is about 15% less than $2zD$ – this effect is illustrated by the solid line in Figure 7, which is an extrapolation of the behaviour in the zone center. In addition the zone boundary spin wave modes for both cubic and bilayer systems are extremely broad in comparison with their energy.

The theory of bilayer manganites presented here shows that the double exchange model can exhibit both of these effects, when quantum corrections are included. However, the minimal model equation (1), as parameterized above, is not sufficient to obtain a quantitative description of the experimental results.

The dominant effect of quantum corrections to the spinwave dispersion of a bilayer DEFM is a substantial downward renormalization of the spin stiffness D, as was noted for a 2D system by Golosov [28]. This means that, to obtain a fit to the dispersion of the bilayer system with quantum effects included, much larger values of the parameters t and $t_\perp$ must be used. The dispersion of the simple DE model we have considered, with quantum effects included, is shown in Figure 7, for parameters chosen to reproduce the spinwave bandwidth at a semi–classical level. Clearly, the overall scale of dispersion is now too small, and t and $t_\perp$ need to be reparameterized. Naively, judging by the renormalization of the spin stiffness. one would need to use a value of t approximately twice as large.

However, this will not help us to explain the measured deviation from nearest neighbour Heisenberg behaviour, because the quantum corrections to the DE model considered have the wrong "sign", as is shown in the inset to Figure 7. The same sign of corrections is seen for this doping in the spinwave theory of the 2D DEFM [17,18]. Therefore including these quantum effects does not improve the fit with experiment. For this reason we will not attempt to reparameterize the model equation (1), and discuss results only for the semi–classical values of t and $t_\perp$ already quoted.

The failure of the minimal model equation (1) to fully explain the spinwave dispersion of $La_{1.2}Sr_{1.8}Mn_2O_7$ is neither very surprising nor very disappointing, given that we have attempted to fit the spin wave dispersion of a complex system with spin charge and lattice degrees of freedom throughout the Brillouin Zone, using only two adjustable parameters. However it is important to ask which of the many simplifications made is to blame for this disagreement with experiment?

A better fit could probably be obtained at a semi–classical level, by substituting a more realistic dispersion for the underlying electrons into the one loop diagrams used to calculate the $\mathcal{O}(1/S)$ spin wave self energy. In tight binding language, each hopping integral t_{ij} has a corresponding DE coupling J_{ij}^{DE} associated with it. The inclusion of t_{ij} beyond nearest neighbours to obtain a more realistic electronic band structure therefore also modifies the form of dispersion of the classically equivalent effective Heisenberg model. Attempts to calculate spin wave dispersion directly from electronic structure suggest that this effect is important, and leads to a softening of zone boundary modes, at least in cubic systems [30].

At a quantum mechanical level, since interactions between spin waves are mediated by density fluctuations of the electron gas, it would be more realistic to use a screened form of the charge susceptibility in which long range interactions were suppressed. We anticipate that this would also tend to enhance the softening of zone boundary modes. The inclusion of leading quantum corrections in $\mathcal{O}(t/J_H)$, likewise leads to a softening of zone boundary spin waves [31,32].

Each of these improvements to the model would involve the introduction of new parameters, which would need to be checked against electronic structure and other experiments. Since the stated aim of this paper is to explore the minimal model equation (1), we will not discuss such refinements further here.

A more interesting possibility to explain the difference between experiment and theory would be that spin waves are coupled to orbital and/or lattice modes, or that disorder leads to non trivial corrections to the spinwave dispersion. We return to these issues below.

The present theory is more successful in explaining the damping at least in a qualitative way. Figure 8 shows the experimentally observed widths of the energy scans as a function of momentum transfer q from zone center to the zone boundary for the acoustic spin excitations of bilayer manganite $La_{1.2}Sr_{1.8}Mn_2O_7$, along with that obtained from the present theory (continuous line). Data measured at different Neutron sources have been plotted together.

The damping which we calculate has a similar momentum dependence to that observed, but is smaller by approximately a factor of four. Some part of the difference in absolute value between theory and experiment can be explained by the fact that, as discussed above, the parameters t and $t_\perp$ were chosen so as to correctly reproduce the spin wave bandwidth at a semi–classical level. Using a more realistic value of t would increase the predicted spinwave damping by a factor of about two.

Our conclusion is that the minimal DE model fails to explain the softening of zone boundary spin waves in $La_{1.2}Sr_{1.8}Mn_2O_7$, but can explain up to about 50% of their

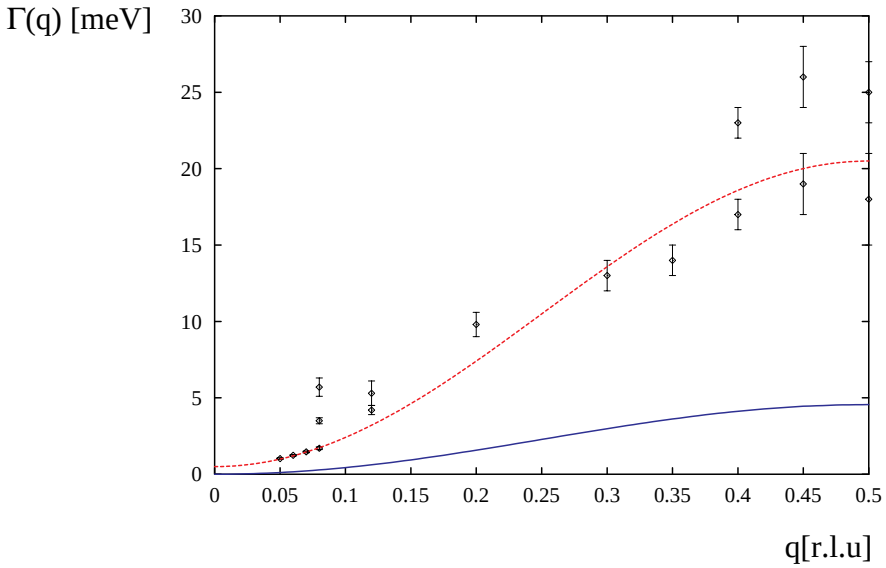

Fig. 8. Damping of acoustic spin wave modes on the line ΓX. Points with error bars – experimental data for $La_{1.2}Sr_{1.8}Mn_2O_7$ taken from [3]; lower solid line – theoretical predicted damping for minimal model with $x = 0.4$, $t = 0.175$ eV, $t = 0.1$ eV. The dashed line is a guide to the eye.

width. Of the refinements to the model discussed above, only the use of a screened charge susceptibility would affect the calculated damping of spin waves, but we do not anticipate that this would lead to a marked increase in their width. We therefore conclude that spin waves in the FM phase of this bilayer manganite are coupled dynamically to another mode, probably of orbital and/or lattice excitations. Such a couplings have been proposed in the context of the cubic manganites – for example to optical phonons [32] or through Jahn Teller active lattice modes to orbital fluctuations [25]. Besides contributing to damping in their own right, a coupling to lattice modes can also lead to a substantial downward renormalization of the semi–classical spinwave dispersion [33]. In this case still larger values of the hopping parameter t would have to be used to fit the data, helping to close the gap between the measured and the calculated spinwave damping.

One further possibility that should also be investigated is the role of disorder, which by mixing spinwaves of different wave number q, also contributes to their width. It has recently been suggested that strong disorder can also lead to non–trivial renormalizations of the spinwave dispersion [34].

5 Conclusions

We have constructed the simplest possible model for ferromagnetism in $La_{1.2}Sr_{1.8}Mn_2O_7$, based on Zener's double exchange mechanism within a one orbital picture for a single bilayer. This model has two adjustable parameters, the intra– and inter-plane hopping integrals t and $t_\perp$. At a semi–classical level it is equivalent to a Heisenberg model with intra– and interplane exchange integral J^{DE} and $J_\perp^{DE}$. The doping dependence of these parameters was discussed, and the predictions of the effective Heisenberg model compared with the results of inelastic Neutron scattering experiments.

As the experiments show departures from simple Heisenberg model behaviour in both the form of dispersion and the scale of damping of the spin waves at low temperatures, we also calculated the leading quantum corrections to spin wave self energies. These arise because of the scattering of spin waves from density fluctuations of the electron gas which are neglected in the semi–classical approximation. We find that the minimal model considered cannot explain the softening of zone boundary spin wave modes, and somewhat underestimates the damping of spin waves, even when quantum corrections are included. This suggests that spin waves are strongly coupled to another low energy mode, presumably related to lattice fluctuations, either by a direct coupling to phonons or an indirect "orbital fluctuation" effect.

It is our pleasure to acknowledge helpful conversations with George Jackeli, Giniyat Khaliullin and Natasha Perkins. This work was in part supported under the visitors program of MPI–PKS (N.S. and F.O.).

Appendix A: Spinwave–electron interaction vertices and self energy corrections at $\mathcal{O}(1/S^2)$

First we give the interaction vertices $V^{1\eta 3\nu}_{2\eta' 4\nu'}$ in Figure 1 and equation (9). There are eight possible channels for

electron–spin wave interaction; these are labeled according to the convention in Figure 1. The coefficients of these vertices are given by

$$\mathcal{V}^{01,03}_{02,04} = \frac{1}{4S}\left[\frac{v^{13}_{24}}{2} + \frac{t_\perp}{8S}\right]$$

$$\mathcal{V}^{\pi 1,\pi 3}_{\pi 2,\pi 4} = \frac{1}{4S}\left[\frac{v^{13}_{24}}{2} - 2t_\perp - \frac{t_\perp}{8S}\right]$$

$$\mathcal{V}^{01,\pi 3}_{02,\pi 4} = \frac{1}{4S}\left[\frac{v^{13}_{24}}{2} + 2t_\perp + \frac{t_\perp}{8S}\right]$$

$$\mathcal{V}^{\pi 1,03}_{\pi 2,04} = \frac{1}{4S}\left[\frac{v^{13}_{24}}{2} - \frac{t_\perp}{8S}\right]$$

$$\mathcal{V}^{01,\pi 3}_{\pi 2,04} = \mathcal{V}^{\pi 1,03}_{02,\pi 4} = \frac{1}{4S}\left[\frac{v^{13}_{24}}{2} + t_\perp\right]$$

$$\mathcal{V}^{\pi 1,\pi 3}_{02,04} = \mathcal{V}^{01,03}_{\pi 2,\pi 4} = \frac{1}{4S}\left[\frac{v^{13}_{24}}{2} - t_\perp\right]. \quad \text{(A.1)}$$

Where the vertex depends on in–plane momenta only through in–plane electronic dispersion

$$v^{13}_{24} = \left[\left(1 - \frac{1}{2S}\right)(\epsilon_{1+3} + \epsilon_{2+4}) - \left(1 - \frac{3}{8S}\right)(\epsilon_1 + \epsilon_2)\right] \quad \text{(A.2)}$$

where $\epsilon_k = -zt\frac{1}{2}(\cos k_x + \cos k_y)$. The fundamental energy scales in the DEFM are set by the kinetic energy of the itinerant electrons, and so it is natural that the electron spin wave scattering vertices are proportional to $t/t_\perp$.

Knowledge of the Hamiltonian equation (6) is sufficient to develop a zero temperature diagrammatic perturbation theory in $1/S$ for the spin wave dispersion of the DE bilayer, up to $\mathcal{O}(1/S^2)$, and to calculate the leading contributions to spin wave damping. The relevant processes are shown in Figure 2. At $\mathcal{O}(1/S)$ only the single loop diagrams a) and b) contribute. These evaluate to give the Heisenberg–model like result equation (12) for the semi–classical spin wave dispersion.

The one loop diagrams also contribute a constant term and a further renormalisation of the classical dispersion at $\mathcal{O}(1/S^2)$, but all new quantum effects arise from the new processes contributing to spin wave self energy at $\mathcal{O}(1/S^2)$, the "watermelon" diagrams shown in Figure 2c–f. The self energy corrections for acoustic modes evaluate to give:

$$\Sigma^{Ic}(\Omega, q) = \frac{1}{(4S)^2}\frac{1}{N^2}\sum_{kq'}\left[\frac{zt}{2}\left(\gamma_k + \gamma_{k+q'} - 2\gamma_{k+q}\right)\right]^2 \times \frac{\theta\left(\xi^0_{k+q'}\right)\theta\left(-\xi^0_k\right)}{\Omega - \omega^0_{q-q'} - \xi^0_{k+q'} + \xi^0_k + \mathrm{i}\delta} \quad \text{(A.3)}$$

$$\Sigma^{Id}(\Omega, q) = \frac{1}{(4S)^2}\frac{1}{N^2}\sum_{kq'}\left[\frac{zt}{2}\left(\gamma_k + \gamma_{k+q'} - 2\gamma_{k+q}\right)\right]^2 \times \frac{\theta\left(\xi^\pi_{k+q'}\right)\theta\left(-\xi^\pi_k\right)}{\Omega - \omega^0_{q-q'} - \xi^\pi_{k+q'} + \xi^\pi_k + \mathrm{i}\delta} \quad \text{(A.4)}$$

$$\Sigma^{Ie}(\Omega, q) = \frac{1}{(4S)^2}\frac{1}{N^2}\sum_{kq'}\left[\frac{zt}{2}\left(\gamma_k + \gamma_{k+q'} - 2\gamma_{k+q}\right) + t_\perp\right]^2 \times \frac{\theta\left(\xi^0_{k+q'}\right)\theta\left(-\xi^\pi_k\right)}{\Omega - \omega^\pi_{q-q'} - \xi^0_{k+q'} + \xi^\pi_k + \mathrm{i}\delta} \quad \text{(A.5)}$$

$$\Sigma^{If}(\Omega, q) = \frac{1}{(4S)^2}\frac{1}{N^2}\sum_{kq'}\left[\frac{zt}{2}\left(\gamma_k + \gamma_{k+q'} - 2\gamma_{k+q}\right) - t_\perp\right]^2 \times \frac{\theta\left(\xi^\pi_{k+q'}\right)\theta\left(-\xi^0_k\right)}{\Omega - \omega^\pi_{q-q'} - \xi^\pi_{k+q'} + \xi^0_k + \mathrm{i}\delta} \quad \text{(A.6)}$$

where we have written out electron energies explicitly and suppressed terms of $\mathcal{O}(1/S^3)$ in the vertex. The corresponding processes for optical spin waves yield:

$$\Sigma^{IIc}(\Omega, q) = \frac{1}{(4S)^2}\frac{1}{N^2}\sum_{kq'}\left[\frac{zt}{2}\left(\gamma_k + \gamma_{k+q'} - 2\gamma_{k+q}\right) + 2t_\perp\right]^2 \times \frac{\theta\left(\xi^0_{k+q'}\right)\theta\left(-\xi^0_k\right)}{\Omega - \omega^\pi_{q-q'} - \xi^0_{k+q'} + \xi^0_k + \mathrm{i}\delta} \quad \text{(A.7)}$$

$$\Sigma^{IId}(\Omega, q) = \frac{1}{(4S)^2}\frac{1}{N^2}\sum_{kq'}\left[\frac{zt}{2}\left(\gamma_k + \gamma_{k+q'} - 2\gamma_{k+q}\right) - 2t_\perp\right]^2 \times \frac{\theta\left(\xi^\pi_{k+q'}\right)\theta\left(-\xi^\pi_k\right)}{\Omega - \omega^\pi_{q-q'} - \xi^\pi_{k+q'} + \xi^\pi_k + \mathrm{i}\delta} \quad \text{(A.8)}$$

$$\Sigma^{IIe}(\Omega, q) = \frac{1}{(4S)^2}\frac{1}{N^2}\sum_{kq'}\left[\frac{zt}{2}\left(\gamma_k + \gamma_{k+q'} - 2\gamma_{k+q}\right) + t_\perp\right]^2 \times \frac{\theta\left(\xi^\pi_{k+q'}\right)\theta\left(-\xi^0_k\right)}{\Omega - \omega^0_{q-q'} - \xi^\pi_{k+q'} + \xi^0_k + \mathrm{i}\delta} \quad \text{(A.9)}$$

$$\Sigma^{IIf}(\Omega, q) = \frac{1}{(4S)^2}\frac{1}{N^2}\sum_{kq'}\left[\frac{zt}{2}\left(\gamma_k + \gamma_{k+q'} - 2\gamma_{k+q}\right) - t_\perp\right]^2 \times \frac{\theta\left(\xi^0_{k+q'}\right)\theta\left(-\xi^\pi_k\right)}{\Omega - \omega^0_{q-q'} - \xi^0_{k+q'} + \xi^\pi_k + \mathrm{i}\delta}. \quad \text{(A.10)}$$

To $\mathcal{O}(1/S^2)$, we can neglect the frequency dependence of the denominator in these expressions and evaluate the leading quantum corrections to the dispersion of optical and acoustic spin wave branches numerically by Monte Carlo integration.

If we restore the frequency dependence of the self energy terms, we can also calculate the imaginary part of each. We can use this to estimate the spin wave damping on the mass shell, by setting the external frequency equal to the semi–classical spin wave dispersion at that wave number, *i.e.* setting $\Omega = \omega_q^{0,\pi}$, and eliminating all terms in the numerator of order spin wave frequencies. The contribution to damping from diagram IId) is, for example:

$$\Gamma^{IId}(\omega_q^\pi, q) = \frac{\pi}{(4S)^2}\frac{1}{N^2}\sum_{kq'}\left[zt_\parallel\left(\gamma_k - \gamma_{k+q}\right) - 2t_\perp\right]^2 \times \theta\left(\xi^\pi_{k+q'}\right)\theta(-\xi^\pi_k)\delta\left(\omega^\pi_q - \omega^0_{q-q'} - \xi^\pi_{k+q'} + \xi^\pi_k\right). \tag{A.11}$$

References

1. *Colossal Magnetoresistance, Charge Ordering, and Related Properties of Manganese Oxides*, edited by C.N.R. Rao, B. Raveau (World Scientific, Singapore, 1998)
2. Yu.A. Izyumov, Yu.N. Skryabin, Physics- Uspekhi **44**, 109 (2001)
3. T. Chatterji, to be published
4. K. Hirota, Y. Moritomo, H. Fujioka, M. Kubota, H. Yoshizawa, Y. Endoh, J. Phys. Soc. Jpn **98**, 3380 (1998)
5. M. Kubota, H. Fujioka, K. Hirota, K. Ohoyama, Y. Moritomo, H. Yoshizawa, Y. Endoh, J. Phys. Soc. Jpn **69**, 1606 (2000)
6. S. Okamoto, S. Ishihara, S. Maekawa, Phys. Rev. B **63**, 104401 (2001)
7. J. Dho, W.S. Kim, H.S. Choi, E.O. Chi, N.H. Hur, J. Phys. Cond. Matt. **13**, 3655 (2001)
8. K. Hirota, S. Ishihara, H. Fujioka, M. Kubota, H. Yoshizawa, Y. Moritomo, Y. Endoh, S. Maekawa, Phys. Rev. B **65**, 64414 (2002)
9. T. Chatterji, P. Thalmeier, G.J. McIntyre, R. van de Kamp, R. Suryanarayanan, G. Dahlenne, A. Revcolevschi, Europhys. Lett. **46**, 801 (1999)
10. T. Chatterji, L.P. Regnault, P. Thalmeier, R. Suryanarayanan, G. Dahlenne, A. Revcolevschi, Phys. Rev. B **60**, R6965 (1999)
11. T. Chatterji, L.P. Regnault, P. Thalmeier, R. van de Kamp, W. Schmidt, A. Hiess, P. Vorderwisch, R. Suryanarayanan, G. Dahlenne, A. Revcolevschi, J. Alloys Compounds **326**, 15 (2001)
12. H. Fujioka, M. Kubota, K. Hirota, H. Yoshizawa, Y. Moritomo, Y. Endo, J. Phys. Chem. Sol. **60**, 1165 (1999)
13. G. Chaboussant, T.G. Perring, G. Aeppli, Y. Tokura, Physica B **276-278**, 801 (2000)
14. T.G. Perring, D.T. Androja, G. Chaboussant, G. Aeppli, T. Kimura, Y. Tokura, Phys. Rev. Lett. **87**, 217201 (2001)
15. C. Zener, Phys. Rev. **82**, 403 (1951)
16. N. Furukawa, J. Phys. Soc. Jpn **65**, 1174 (1996)
17. N. Shannon, A. Chubukov, J. Phys. Cond. Matt. **14**, L235 (2002)
18. N. Shannon, A. Chubukov, Phys. Rev. B **65**, 104418 (2002)
19. N. Shannon, *Introductary lecture given at VI Vietri Training Course, October 2001*, `cond-mat/0203156`
20. N. Shannon, J. Phys. Cond. Matt. **13**, 6371 (2001)
21. S. Rosenkranz, R. Osborn, L. Vasiliu-Doloc, J.F. Mitchell, J.W. Lynn, S.K. Sinha, J. Appl. Phys. **87**, 5816 (2000)
22. P.K. deBoer, R.A. de Groot, Phys. Rev. B **60**, 10758 (1999)
23. E.L. Nagaev, *Physics of Magnetic Semiconductors* (Mir, Moscow, 1979)
24. E.L. Nagaev, Phys. Rev. B **58**, 827 (1998)
25. G. Khaliullin, R. Kilian, Phys. Rev. B **61**, 3493 (2000)
26. T. Chatterji, R. Schneider, J.-W. Hoffmann, D. Hohlwein, R. Suryanarayanan, G. Dahlenne, A. Revcolevschi, Phys. Rev. B **65**, (2002)
27. Since completing this work we have become aware of a mean field theory calculation of the variation of J^{DE} and $J_\perp^{DE}$ as function of doping for a two orbital model, G. Jackeli, N.B. Perkins, Phys. Rev. B **65**, 212402 (2002)
28. D. Golosov, Phys. Rev. Lett. **84**, 3974 (2000)
29. H.Y. Hwang, P. Dai, S-W. Cheong, G. Aeppli, D.A. Tennant, H.A. Moo, Phys. Rev. Lett. **80**, 1316 (1998)
30. I.V. Solovyev, K. Terakura, Phys. Rev. Lett. **82**, 2959 (1999)
31. F. Mancini, N.B. Perkins, N.M. Plakida, Phys. Lett. A **284**, 286 (2001)
32. N. Furukawa, J. Phys. Soc. Jpn **68**, 2252 (1999)
33. M. Hohenadler, D.M. Edwards, J. Phys. Cond. Matt. **14**, 2547 (2002)
34. Y. Motome, N. Furukawa, preprint, `cond-mat/0203041`